

ELECTROSTATIC DISPERSION AND
EVAPORATION OF CLUSTERS OF DROPS OF
HIGH-ENERGY FUEL, FOR '1' CONTROL,

J. Bellan and K. Harstad

Jet Propulsion Laboratory

California Institute of Technology

4800 Oak Grove Drive

Pasadena, CA. 91109 USA

Corresponding author: J. Bellan

Tel: (m) 354 6959

FAX: (818) 393 1633

e-mail: jbellan@zenith.jpl.nasa.gov

1 Preferred oral presentation

Colloquium topic: Spray Combustion

Word count: 5553

(w: 229x14: 3206; eqs: '(X2?)= 147; tpls: 200; figs: 4x: 900-14x300: 2,000)

Abstract

A model is presented for the electrostatic dispersion of a polydisperse cluster of evaporating drops embedded into an inviscid vortex. Results from this model obtained for dense clusters of drops show that electrostatic dispersion decreases the mass fraction of the evaporating compound as well as the gas density inside the cluster. Since the sooting tendency of a fuel is an increasing function of the partial density of the fuel vapor through coagulation, it is inferred that electrostatic charging decreases the sooting tendency. Results show that the sooting tendency is a monotonically decreasing function of the charge. By using this model for different fuels, it is shown that sooting of a fuel is associated with two competing characteristic times: that of drop dispersion and that of drop evaporation. It is also shown that the drop evaporation time is directly related to the latent heat of the fuel thereby providing a simple way to relate sooting propensity to fuel-specific properties.

1 Introduction

This study investigates the potential of electrostatic liquid drop charging to disperse the drops of a spray in order to avoid the creation of the fuel-rich-vapor regions where soot forms. Observations by Sangiovanni[1] of streams of burning drops showed that the soot emission index decreases monotonically with the spacing between drops for a variety of fuels and oxygen mass fractions in the surrounding gas. Since in Sangiovanni's study[1] it is only the effect of drop spacing in a single direction that has been investigated, those results underestimate the benefit of drop dispersion in a real spray where a drop is surrounded by other drops in all directions. Electrostatic drop dispersion could be combined with fluid mechanical methods, such as creation of turbulent vortical structures, in order to further mitigate soot formation.

The specific focus here is on several potential fuels with interesting high-energy characteristics. The high-energy of these fuels is stored as strain energy in internal molecular bonds. The goal of the present study is to explore the fuel specific electrostatic and fluid mechanical dispersion features of a variety of potential fuels. A difficulty in pursuing this work arises from the fact that although high-energy fuels have been synthesized, they have not necessarily been purified so that their thermophysical properties are not available. Thus, strategies were developed in the course of this study to calculate *all* thermophysical properties of these potential high-energy fuels starting from a single known property. Fuel properties evaluation is described in detail elsewhere [2] and is summarized in Table 1. The representative fuels considered here are benzvalene (BV), C_6H_6 ; quadricyclane (QUAL), C_7H_8 ; and di-

hydrobenzvalene (DIII 3V), C_6H_8 . The respective strain energies of these hydrocarbons are 81.3 kcal/mole, 78.7 kcal/mole and 80.0 kcal/mole. Although the strain energy of these fuels is only about one half that of cubane, which is 161 kcal/mole, they have the advantage of being directly usable as all of them are liquids and some are stable and blendable with other compounds. In contrast, cubane is a solid that is too crystalline[3] and insufficiently blendable with other hydrocarbons[3]; even when mixed with liquid compounds to form a slurry that can be atomized and burned, it does not participate in combustion and instead accumulates in the drops[4].

2 Electrostatic Dispersion Model

2.1 The electrostatic dispersion model

The configuration modeled is that of a cluster of drops such as observed by many investigators[5], [6], [7], [8], [9], [10]. This configuration of a polydisperse cluster of drops embedded into an axisymmetric, in finite, inviscid vortex where it evaporates and is centrifuged is described in detail elsewhere[11]. The model accounts for interaction among drops through the concept of a "sphere of influence" [11] and includes the two-way coupling between drops and gas in the form of drag as the drop Reynolds number, Re_d , based upon the slip velocity and the drop size is $0(1) - 0(10)$. Since the model is described in detail in [11], here it is only the modification due to the addition of electrostatic effects that is explained. One important feature of this model is that the initial drop size distribution is partitioned into initial-size classes which become identity classes for the drops. Each initial-size class is followed in its own system of coordinates, r_j , as the drops disperse and evaporate. An additional system of coordinates is used for the gas inside the cluster, r_c .

The change of the radial force on a drop of initial-size class j , F_{drj} , due to an electrostatic charge q_{dj} is

$$\delta F_{drj} = q_{dj} E_r = m_{dj} \delta(du_{drj}/dt) \quad (1)$$

where E_r is the radial electric field, m_{dj} is the mass of the drop, u_{drj} is the drop velocity in the radial direction and t is the time. This is a new term to be added to the radial component of the momentum equation. The value of E_r is found from Poisson's equation

$$\nabla \cdot \vec{E} = \rho_{ch}/\epsilon_0 \quad (2)$$

where ρ_{ch} is the charge density and ϵ_0 is the permittivity of free space. Eq.2 is expressed in terms of the drop number density, n_j , for each initial-size class j , as follows

$$(1/r) \partial(r E_r) / \partial r = (1/\epsilon_0) \sum_{j=1}^{JT} q_{dj} n_j \quad (3)$$

where JT is the total number of initial-size classes. Practically, this formulation is implemented into the computer code by following the ring discretization procedure explained in Harstad and Bellan[11] and thus

$$\Delta_k(r E_r) = [1/(2\pi\epsilon_0)] \sum_{j=1}^{JT} q_{dj} N_{cj}^{(k-1/2)} \quad (4)$$

where $N_{cj}^{(k-1/2)} = 2\pi \int_{r_c^{(k-1)}}^{r_c^{(k)}} n_j r dr$ is the number of drops per unit vortex length for initial-size class j , $\Delta_k V = V[r_c^{(k)}] - V[r_c^{(k-1)}]$ where V is an arbitrary variable and $r_c^{(k)}$ is the discretization. The electrostatic energy is not transformed into heat or dissipated. It is transformed into drop kinetic energy.

2.2 The Rayleigh limit

Rayleigh has shown that a charged drop cannot maintain its integrity for increasingly high charges. For a given charge, the minimum radius for which a drop can maintain its integrity is called the Rayleigh limit. This phenomenon is the result of the competing surface tension forces which tend to maintain the drop integrity and the electrostatic forces which tend to pull the drop apart. The total drop energy is the sum of two terms: the surface energy $W_o^d = 4\pi\sigma R_d^2$, and the local electrostatic energy per drop $W_E^d = 0.5\epsilon_0 \int E^2 dV = q_d^2 / (8\pi\epsilon_0 R_d)$. The total energy is minimized at the Rayleigh radius

$$R_{d, Ray} = [q_d^2 / (64\pi^2 \epsilon_0 \sigma)]^{1/3} \quad (5)$$

which is calculated from $[\partial(W_o^d - W_E^d) / \partial R_d](R_{d, Ray}) = 0$. Since evaporating drops maintain their charge, eventually they reach a size at which they split forming siblings; this effect has been studied by Kelly [1-2] who showed that, inexplicably, at the Rayleigh limit the drops split into 7 siblings each inheriting about 14% of the initial charge and having for radius about 52% of the Rayleigh radius.

Previous results obtained with a model of uncharged drops [1-1] showed that due to the larger gas temperature at the cluster inner and outer boundaries, the drop size decreases faster at those locations. Thus, if the Rayleigh limit is reached, it is first reached at either one of the cluster boundaries. In the present model the drops are followed up to the Rayleigh limit; further drop splitting which is beneficial because it provides secondary atomization is not modeled. If the Rayleigh limit is reached by drops at the inner boundary of the cluster, the computation is stopped because the model does not describe the complex and unknown splitting process, and the drops located at larger radial coordinates would be affected by such important changes. These situations are not considered to be of interest. If the Rayleigh limit

is reached at the outer cluster boundary, the calculation is pursued and output of the drops having reached the Rayleigh limit are further ignored. This does not affect electrostatically the drops at smaller radial coordinates. It is assumed that because of the small drop size after drop splitting, the dynamic and thermodynamic effects are also small.

2.3 Relation between drop radius and drop charge

A drop may be endowed with a different quantity of electrostatic charge according to the method used to charge the drop. Using the electrostatic spray triode, Kelly showed that the maximum charge that could be given to a drop was

$$|q_d|_{\max} = 7.36 \times 10^{-11} R_d^0 \text{ coul} \quad (6)$$

This is an empirical relationship. In the present calculations, the charge is chosen to be a fraction of this maximum charge according to Eq. 6. Other possibilities could be considered as well, such as a charge proportional to $(R_d^0)^2$, although there is currently no data leading to such a relationship.

3 Results

In order to understand the separate contributions of gas irrotational motion, gas solid body rotation and electrostatic dispersion, results were here obtained for clusters of drops embedded into vortices having only irrotational motion. The effects of the solid body rotation will be investigated at a later date.

Two sets of results were obtained as described in the following. The purpose of the first set is to allow the study of electrostatic effects as the drops charge is gradually increased.

The second set of results focuses on the fuel-specific behavior of the cluster when the drops are uncharged or charged

3.1 Effect of electrostatic charge on the drops

To study the effect of the electrical charge on the drops, I3V was chosen as a representative compound. The initial conditions were chosen so as to prevent the inner drops from reaching the Rayleigh limit before the outer drops and thereby destroy the integrity of the cluster model; thus, calculations were performed with a relatively low value of the initial far field gas temperature. Constant C_1 in the Nusselt number correlation describing heat transfer to the cluster [11] is 0.5, $C_T = \mu_T Pr_g / (\rho_g r_c \| \bar{u}'_s \|)$ is a constant quantifying the additional viscous contributions due to small scale turbulence [11] where μ_T is the turbulent viscosity, the average slip velocity is $\bar{u}'_s = \sum_j \bar{u}'_{sj} N_{cj} / \sum_j N_{cj}$, and the characteristic time for the increase of $T'_{g\infty}(t)$ is 6×10^{-3} s [11] so that $T'_{g\infty}(t) = T'_{g\infty} [1 - t / (6 \times 10^{-3})]$. This $T'_{g\infty}(t)$ variation simulates the motion of the vortex through an increasing temperature region. The cluster is composed of a binary size distribution (see Fig. 1 caption) and

$$n_j^0(r^0) = N_{cj}^0 A_{\beta_j} \left\{ (r^0 - r_{in,j}^0) / [\alpha_j (r_{out,j}^0 - r_{in,j}^0)] \right\}^{\beta_j} \exp \left\{ -\beta_j (r^0 - r_{in,j}^0) / [\alpha_j (r_{out,j}^0 - r_{in,j}^0)] \right\} \quad (7)$$

where $r_{in,j}^0 = b_{ij} R_c^0$, $0 \leq b_{ij} \leq 1$; $r_{out,j}^0 = b_{oj} R_c^0$, $b_{ij} < b_{oj} \leq 1$; R_c^0 is an initial cluster characteristic dimension and the value of A_{β_j} is found by requiring that $2\pi \int_{r_{in,j}^0}^{r_{out,j}^0} n_j^0 / N_{cj}^0 r dr = 1$. $r_{in}^0 = \min_j (r_{in,j}^0)$ and $r_{out}^0 = \max_j (r_{out,j}^0)$ are respectively the inner and outer cluster boundaries. The value of β_j is specified between 0 and ∞ . Other initial conditions are the initial air/fuel mass ratio, Φ^0 , the initial gas pressure, the initial drop surface temperature, T_{gs}^0 , the initial interstitial gas temperature, T_{gi}^0 , R_c^0 , $A_{g\theta}^0$ ($u_{g\theta}^0 = A_{g\theta}^0 / r^0$ is the initial tangential gas velocity), and the drop velocities. All these values are given in Fig. 1 caption. u_{gi}^0 , the

initial radial gas velocity is calculated from the energy equation[11]. Pr_g is chosen to be 0.8.

Results displayed in Figs. 1-4 show the effect of the drop charge. Calculations were performed with 0.00, 0.25, 0.50 and 0.75 of the maximum initial charge allowed per drop according to Eq.6. Charging the drops with 0.50 of the maximum charge increases drop dispersion approximately by a factor of 2 and decreases the evaporation time to less than 50%. The effect of the charge is to increase the velocities by approximately a factor of 10 and to reduce the nonuniformities of the dependent variables as the cluster expands much faster and the drop number densities decrease. The consequence of these changes is to reduce the mass fraction of the evaporated compound, Y_{Fi} , and the interstitial gas density, ρ_{gi} . Since $s \ll 1$, particle inception has been successfully modeled as a coagulation process[13] which strongly depends on fuel partial density through the quantity of critical molecular size necessary to initiate the process, this reduction is indicative of tendency not to form soot. Coagulation is only weakly dependent upon temperature[14], and thus the slight variations of T_{gi} with charge shown in Fig. 4 do not affect this conclusion. The results show that soot reduction is increased with increasing charge although the largest variation is from uncharged to slightly charged (25%) drops.

An interesting observation is that in the absence of charge it is the largest initial-size-class which is preferentially centrifuged, whereas when using Eq.6, it is the smallest initial-size-class which is preferentially centrifuged. The variation of the total drop number density distribution, n , towards the outer cluster boundary (Fig. 1) reflects the fact that it is the less numerous, larger initial-size-class which is found at the outer boundary when drops are uncharged, whereas when the drops are charged it is the more numerous, smaller initial-size-class which prevail at that location. Since the small drops heat up faster, and thus evaporate faster, this preferential centrifuging promotes mixing and thus provides an additional benefit

from electrostatic charging.

3.2 Fuel-specific effects for uncharged and charged clusters of drops

For each of the three fuels above, several calculations were performed. When at fixed Φ^0 , $T_{g\infty}^0$ is the same for two different fuels, n^0 is different because the liquid densities are different; thus, it is the effect of the liquid density that is studied. When results are compared for calculations having identical n^0 and $T_{g\infty}^0$ for different fuels, it is the effect of Φ^0 that is studied. Finally, for a given compound, when $T_{g\infty}^0$ is increased at fixed Φ^0 , n^0 varies because the initial gas density in the far field, $\rho_{g\infty}^0$, varies since the initial pressure is maintained constant. r_{in}^0 and r_{out}^0 as well as the functional form of the initial distributions Eq. 7 are maintained constant for all the calculations. In all the calculations conducted here there is no fuel vapor in the far field.

Results obtained with uncharged clusters of BV show that, as expected, when $T_{g\infty}^0$ is smaller, n^0 is larger, and evaporation is slower. At fixed $T_{g\infty}^0$, evaporation is faster when Φ^0 is larger because the cluster is leaner and more dilute.

Calculations performed with uncharged drops show that at the same Φ^0 and $T_{g\infty}^0$, n^0 is larger for QUAID than for BV generating a stronger coupling to the gas, as illustrated in Figs 5-8. The larger drop momentum promotes earlier dispersion and higher evaporation rates for QUAID. For BV, the cluster stays denser in its core and evaporation is hindered when compared to QUAID. The fuel vapor mass fraction in the core of the cluster is larger for QUAID, but since the mass fraction has a different reference point in the two cases, it is difficult to draw salient conclusions. of interest is the fact that the (T°C) velocity angle (Fig.8) and Re_d are both larger for BV, for both initial-size classes, although the drop radial and tangential velocities, u_{dr} and $u_{d\theta}$ respectively, are smaller for BV. This is consistent

with the fact that the drops take longer to evaporate (because they stay longer in a dense configuration) although the latent heats are similar and the normal boiling point, T'_{bn} , of BV is lower than that of QUAD.

Comparisons of results from calculations made for the three fuels with identical Φ^0 and $T'_{g\infty}$ reveal that the cluster of DHBV drops evaporates faster, and thus expands less, than that of QUAD because it is more dilute and the latent heat is also smaller. Due to the lower latent heat, although the cluster of DHBV is denser than that of BV, evaporation is faster for 11111 BV drops; thus, there is less time for expansion for the cluster of DHBV drops. Consistent with the decreased expansion and higher n_0 , the gas tangential velocity decreases much faster for DHBV although the gas radial velocity remains larger. This interpretation is supported by the results from the drop velocities. For both initial-size classes the velocity angle is much larger for 1111 BV (Fig. 8) indicating that expansion occurs at a higher rate. The resulting Y_{Fi} and ρ_{gi} are highest for DHBV due to the smaller expansion when compared to QUAD and due to the combined effect of smaller expansion and smaller total number of drops. The conclusion from these calculations with uncharged drops is that at identical Φ^0 and $T'_{g\infty}$, the fuel most prone to form soot would be DHBV.

Thus, it appears that the propensity to soot formation can be explained in terms of two competing characteristic times, that for drop dispersion and that for drop evaporation; the propensity to soot formation increases with the ratio of the former to the latter. The characteristic time for drop evaporation is determined by the latent heat because the clusters of drops are dense during most of their evaporation and thus drops compete for available heat. Inspection of properties displayed in Table 1 and the faster evaporation time for DHBV shows that this interpretation is correct. Electrostatic charging reduces the drop dispersion characteristic time (Figs. 5-8) and accordingly reduces Y_{Fi} and ρ_{gi} . Although it appears that

the Y_{Fi} reduction is similar for the same charge (Fig. 6), interestingly, the ρ_{gi} reduction is greater for DHBV (Fig. 7) indicating that it is for the compound most prone to sooting that electrostatic charging; is I-nest beneficial.

At the same n^0 and n_j^0 , where j represents the initial-size class, Φ^0 is smaller for BV than for QUA1). The larger fuel mass for the calculation with QUA1) results in more centrifugation and drop dispersion at a given time. The evaporation time for BV is again considerably longer than for QUA1).

Comparisons of results from calculations made for the three fuels with identical N^0 , n_0 , n_j^0 and $T_{g\infty}^0$ reveal that it is again the cluster with DHBV drops which evaporates fastest. despite the fact that the cluster of QUA1) drops is leaner. This is again due to the much lower latent heat of evaporation for DHBV than for BV and QUA1). Consistent with the much lower evaporation time, the drop velocity angle and the cluster expansion are smallest. This is somewhat different from the situation when Φ^0 was identical because in that case the velocity angle was the largest indicating the largest expansion rate. Here the expansion rate is smallest as both u_{drj} and $u_{d\theta j}$ have the lowest values for DHBV. The combination of the smallest expansion and highest evaporation rate produces again the largest values for the mass fraction of the evaporated compound for drops of DHBV, leading again to the conclusion that it is DHBV that will be the most prone to sooting.

4 Summary and Conclusions

A model of electrostatic dispersion of a polydisperse cluster of drops in a vortex has been developed and exercised both with and without charge for three potential high-energy fuels in order to determine fuel-specific properties related to soot formation. Since some of these fuels

have been synthesized but not necessarily purified, their properties have not been measured. Thus, in some cases, all properties of these fuels had to be estimated using well-established methods or using new methods which had to be created to estimate the missing properties.

This study identifies which high-energy fuels are more prone to soot formation based upon their specific properties. When evaporation is faster than drop dispersion, fuel rich vapor pockets form inside the cluster of drops; these are the precursors to soot. Results show that evaporation is controlled by the latent heat when the drops are in a dense configuration. When drops are charged, the additional dispersion due to the electrostatic form increases the cluster volume and enhances heat transfer with the cluster surroundings, decreases the drop number density and promotes evaporation. The result is a reduction of the mass fraction of the evaporated compound and the gas density inside the cluster, despite the faster evaporation. For initial electric charges proportional to the drop size, the smaller drops are preferentially dispersed. Since these are the drops which evaporate faster, this preferential dispersion promotes mixing and thus provides an added benefit.

The results presented here were obtained for drops and gas experiencing only irrotational motion. The effect of added solid body rotation will be investigated in the near future.

Acknowledgement

This research was carried out, at the Jet Propulsion Laboratory, California Institute of Technology, under a contract with the National Aeronautics and Space Administration (NASA), and under sponsorship from the Office of Naval Research, with Dr. Gabriel Roy acting as technical monitor through an interagency agreement with NASA.

References

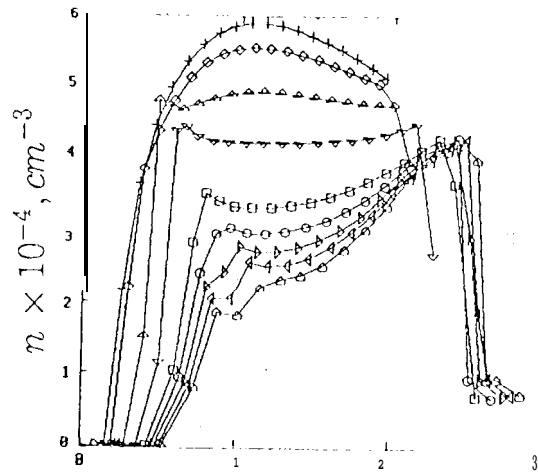
- [1] Sangiovanni, J. J. and Liscinsky, D. S., *Twentieth Symposium (International) on Combustion*, 1985, The Combustion Institute, pp. 1063-1073
- [2] Bellan, J., *8th ONR Propulsion Meeting*, 1995, pp. 168-182
- [3] Moriarty, R. M., private communication, 10/28/94
- [4] Law, C. K., *7th ONR Propulsion Meeting*, 1994, pp.110-116
- [5] Mao C-I., Occhle, V and Chigier, N. A., *Drop Size Distribution and Air Velocity Measurements in Air Assist Swirl Atomizer Sprays*, Central/Western States Meeting/The Combustion Institute, 1985
- [6] Allen, M. G. and Hanson, R. K., *Twentyfirst Symposium (International) on Combustion*, The Combustion Institute, 1987, pp. 1755-1762
- [7] Rudoff, R. C., Brena de la Rosa, A., Sankar, S. V. and Bachalo, W. D., *27th Aerospace Sciences Meeting*, paper AIAA-89-0052
- [8] McDonell, V. G., Adachi, M. and Samuelsen, G. S., *Combust. Sci. and Tech.* 82:225-248 (1992)
- [9] McDonell, V. G., Adachi, M. and Samuelsen, G. S., *Atomization and Sprays* 4:411-436 (1993)
- [10] Nakabe, K., Mizutani, Y., Akamatsu, F. and Fujoka, H, *Atomization and Sprays* 4(5):485-500 (1994)

- [11] Harstad, K. and Bellan, J., "Behavior of a 101 ydisperse Cluster of 1 Drops Evaporating in an Inviscid Vortex", submitted for publication
- [12] Kelly, A. J., *J. of Inst. of Energy* 51 (431):312-320 (1984)
- [13] Santoro, R. J., *Soot Formation: A View of Our Current Understanding*, invited paper , Eastern States Meeting, The Combustion Institute, 1995
- [14] Santoro, R. J., private communication, 12/1/1995

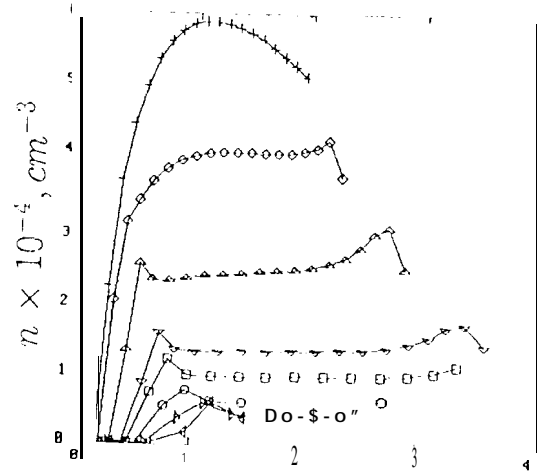
Symbol	Benzvalene	Quadricyclane	Dihydrobenzvalene
$\Phi_{stoch} \equiv$ air mass/fuel mass	13.2	13.4	13.7
strain energy, kcal/mole	81.3	78.7	80.0
w , ~./mole	78.12	92.14	80.14
T_{bn} , K	353	382	344
I_{bn} , cal/g	96.90	96.85	74.50
ΔC_p , cal/(gK)	6.8×10^{-2}	1.48×10^{-3}	0 (assumed)
ρ_l , g/cm ³	0.879	0.7	0.71
C_{pl} , cal/(gK)	0.415	0.36	0.43'2
μ_l , g/(cms)	0.392×10^2	0.316×10^{-2}	0.35×10^2 (assumed)
$D_{ml}(Le_l = 10)$, cm ² /s	0.995×10^{-4}	0.999×10^{-4}	0.978×10^{-4}
λ_l , cal/(gK)	3.63×10^{-4}	2.67×10^{-4}	3×10^{-4}
C_{pg}	0.37	0.435	0.437

Table 1: Properties of high-energy fuels

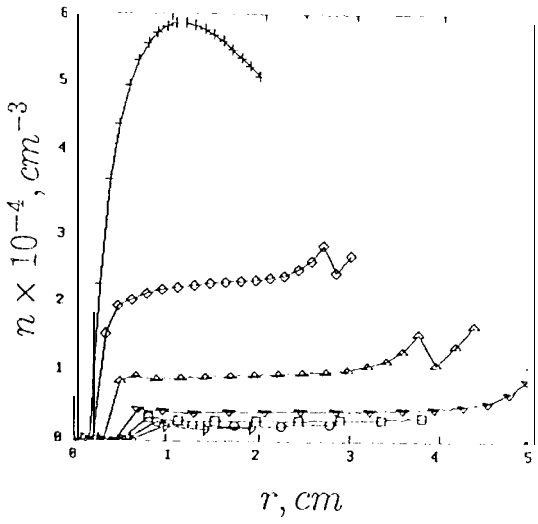
1. Figure 1 Decay of the total drop number density for benzvalene versus the radial coordinate at various times. The drops in the cluster are charged with the following percentages of the maximum charge: 0% (a); 25% (b); 50% (c); 75% (d). Initial conditions are: $\Phi^0 = 0.314$, $T_{g\infty}^0 = T_{gs}^0 = 600K$, $T_{gs}^0 = 300K$, $R_1^0 = 2 \times 10^{-3}cm$, $R_2^0 = 2.5 \times 10^{-3}cm$, $\max_{r_1^0}(n_1^0) = 10^4cm^{-3}$, $\max_{r_2^0}(n_2^0) = 3 \times 10^3cm^{-3}$, $\alpha_1 = \alpha_2 = 0.5$, $\beta_1 = \beta_2 = 0.5$, $R_c^0 = 2cm$, $b_{i1} = b_{i2} = 0.1$, initial drop acceleration for both classes is 20 cm/s, $u_{g\theta}^0 = 100/r_c^0 cm/s$, $C_T = 0.05$. Curves with symbols (-), (0), (Δ) and (∇) are for identical times on all figures and the respective times are $8.37 \times 10^{-5}s$, $1.75 \times 10^{-3}s$, $3.48 \times 10^{-3}s$, and $5.94 \times 10^{-3}s$. In all figures the list of symbols in order of increasing times is: (+), (\diamond), (Δ), (∇), (\square), (\circ), (D), (\triangleleft), ($\hat{\square}$), and (\sqcup).
2. Figure 2 Increase of the interstitial mass fraction of benzvalene vapor with time versus the radial coordinate. The drops in the cluster are charged with the following percentages of the maximum charge: 0% (a); 25% (b); 50% (c); 75% (d). Same initial conditions as in Fig. 1. Curves with symbols (-), (0), (Δ) and (∇) are for identical times on all figures.
3. Figure 3 Increase of the interstitial gas density in the cluster with time versus the radial coordinate. The drops in the cluster are charged with the following percentages of the maximum charge: 0% (a); 25% (b); 50% (c); 75% (d). Same initial conditions as in Fig. 1. Curves with symbols (-), (0), (Δ) and (∇) are for identical times on all figures.
4. Figure 4 Temperature evolution with time versus the radial coordinate. The drops in the cluster are charged with the following percentages of the maximum charge: 0% (a); 25% (b); 50% (c); 75% (d). Same initial conditions as in Fig. 1. Curves with symbols (+), (0), (Δ) and (∇) are for identical times on all figures.
5. Figure 5 Decay of the total drop number density for benzvalene (a), quadricyclane (b), and dihydrobenzvalene (c) with time versus the radial coordinate. Comparisons are made between drops charged with 0% (left figures) and 25% (right figures) of the maximum charge. Same initial conditions as in Fig. 1. Only the curves with symbol (∇) are for identical times on all figures corresponding to $3.48 \times 10^{-3}s$.
6. Figure 6 Increase of the interstitial mass fraction for benzvalene (a), quadricyclane (b), and dihydrobenzvalene (c) with time versus the radial coordinate. Comparisons are made between drops charged with 0% (left figures) and 25% (right figures) of the maximum charge. Same initial conditions as in Fig. 1. Only the curves with symbol (∇) are for identical times on all figures.
7. Figure 7 Increase of the interstitial gas density for benzvalene (a), quadricyclane (b), and dihydrobenzvalene (c) with time versus the radial coordinate. Comparisons are made between drops charged with 0% (left figures) and 25% (right figures) of the maximum charge. Same initial conditions as in Fig. 1. Only the curves with symbol (∇) are for identical times on all figures.
8. Figure 8 Variation of the drop velocity angle for initial-size-class-1 for benzvalene (a), quadricyclane (b), and dihydrobenzvalene (c) with time versus the radial coordinate. Comparisons are made between drops charged with 0% (left figures) and 25% (right figures) of the maximum charge. Same initial conditions as in Fig. 1. Only the curves with symbol (∇) are for identical times on all figures.



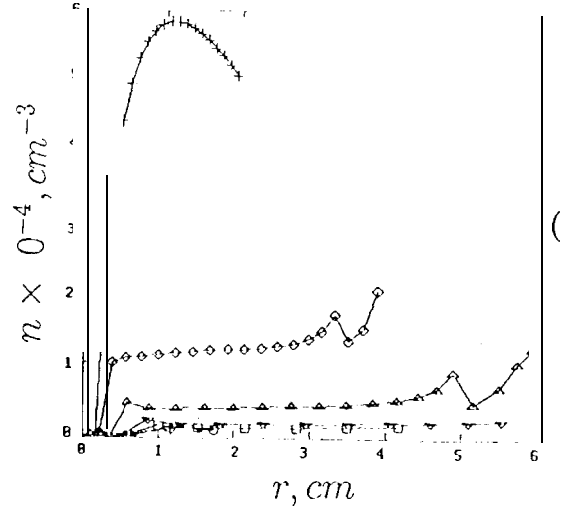
(a)



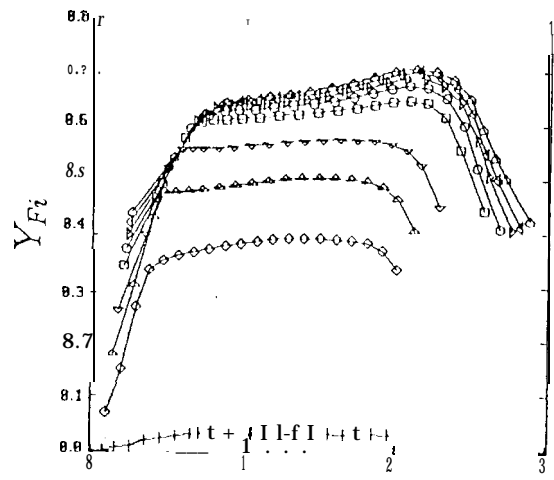
(b)



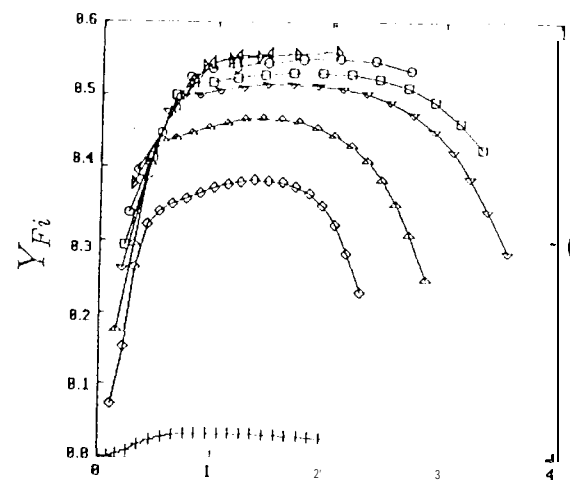
(c)



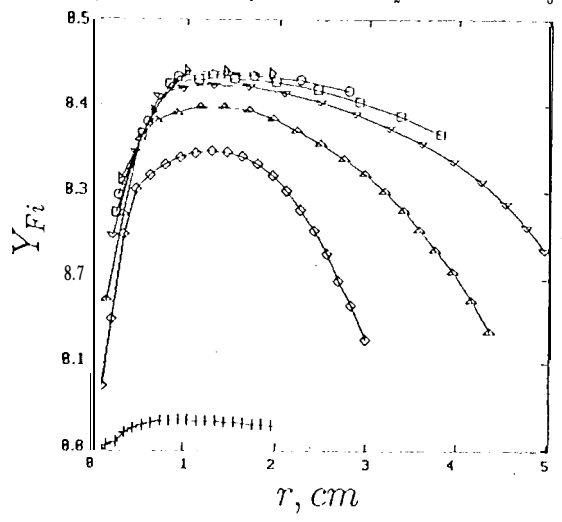
(d)



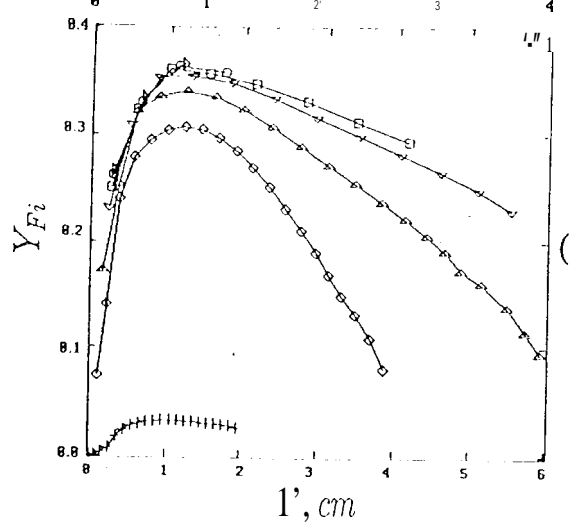
(a)



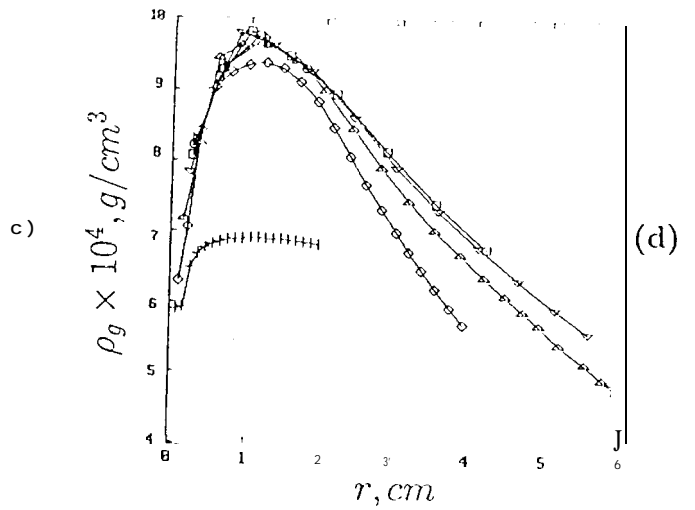
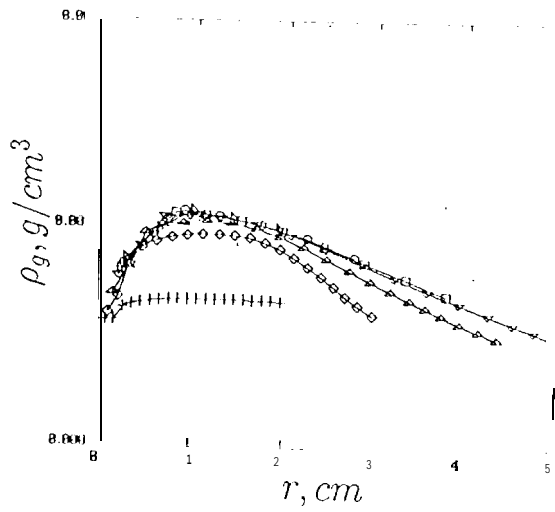
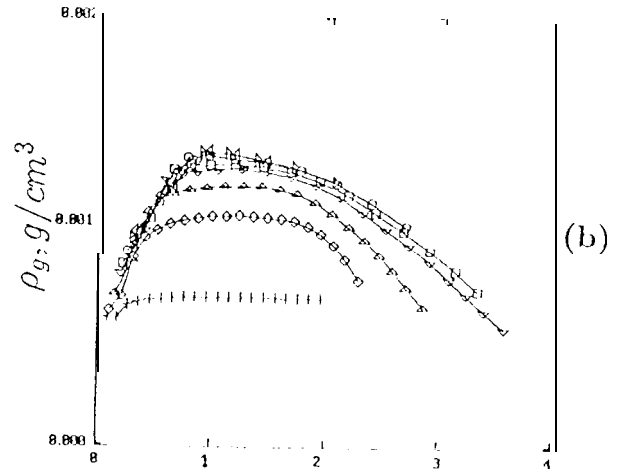
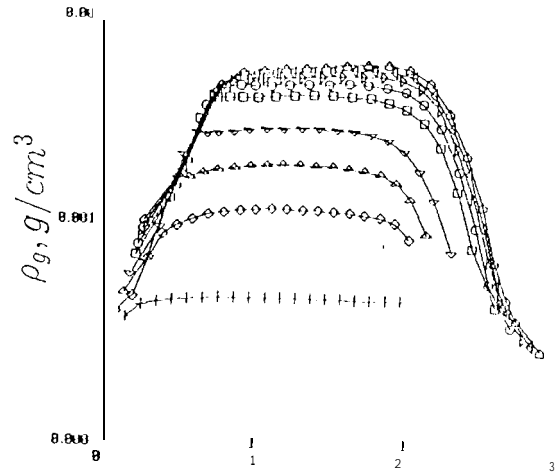
(b)

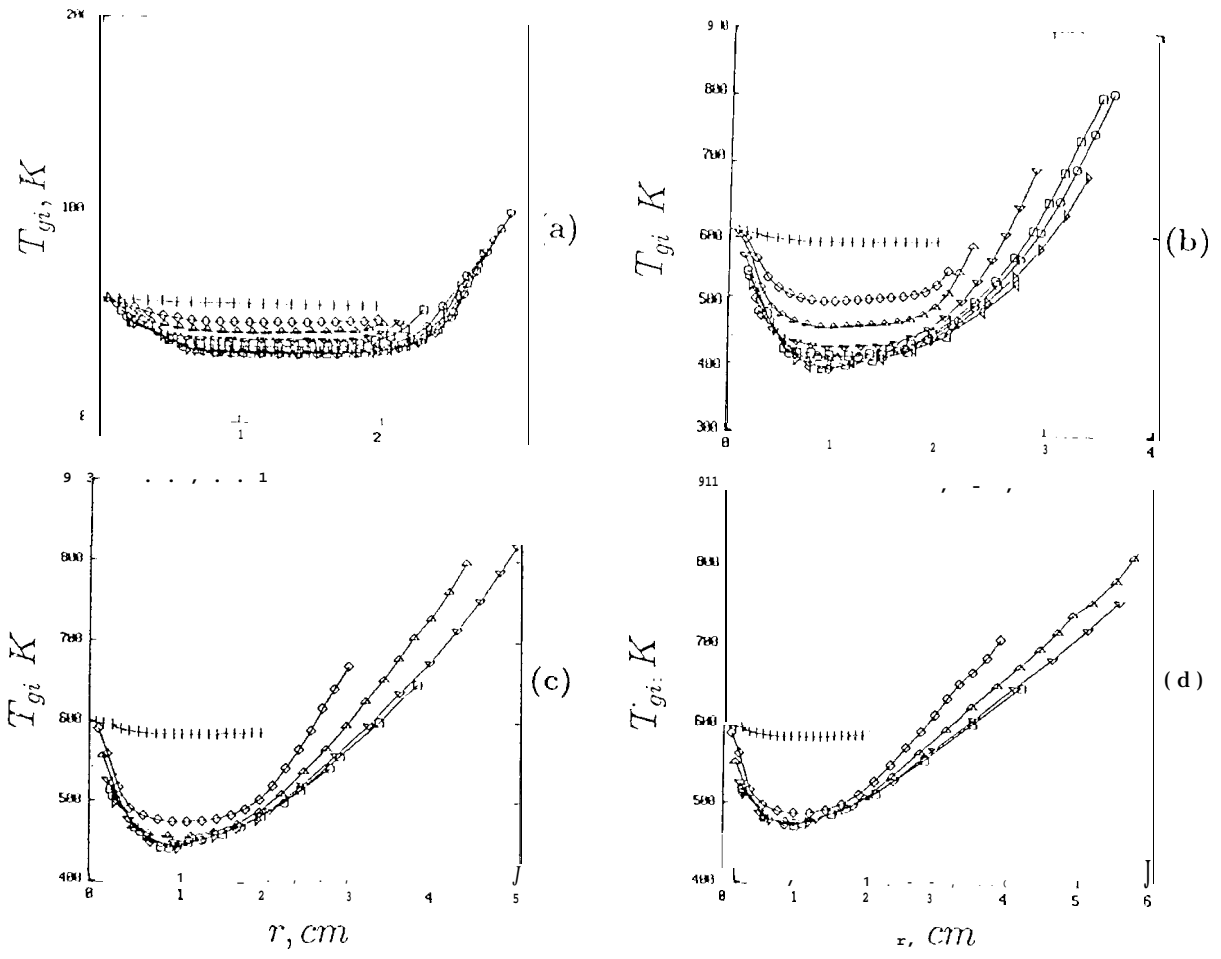


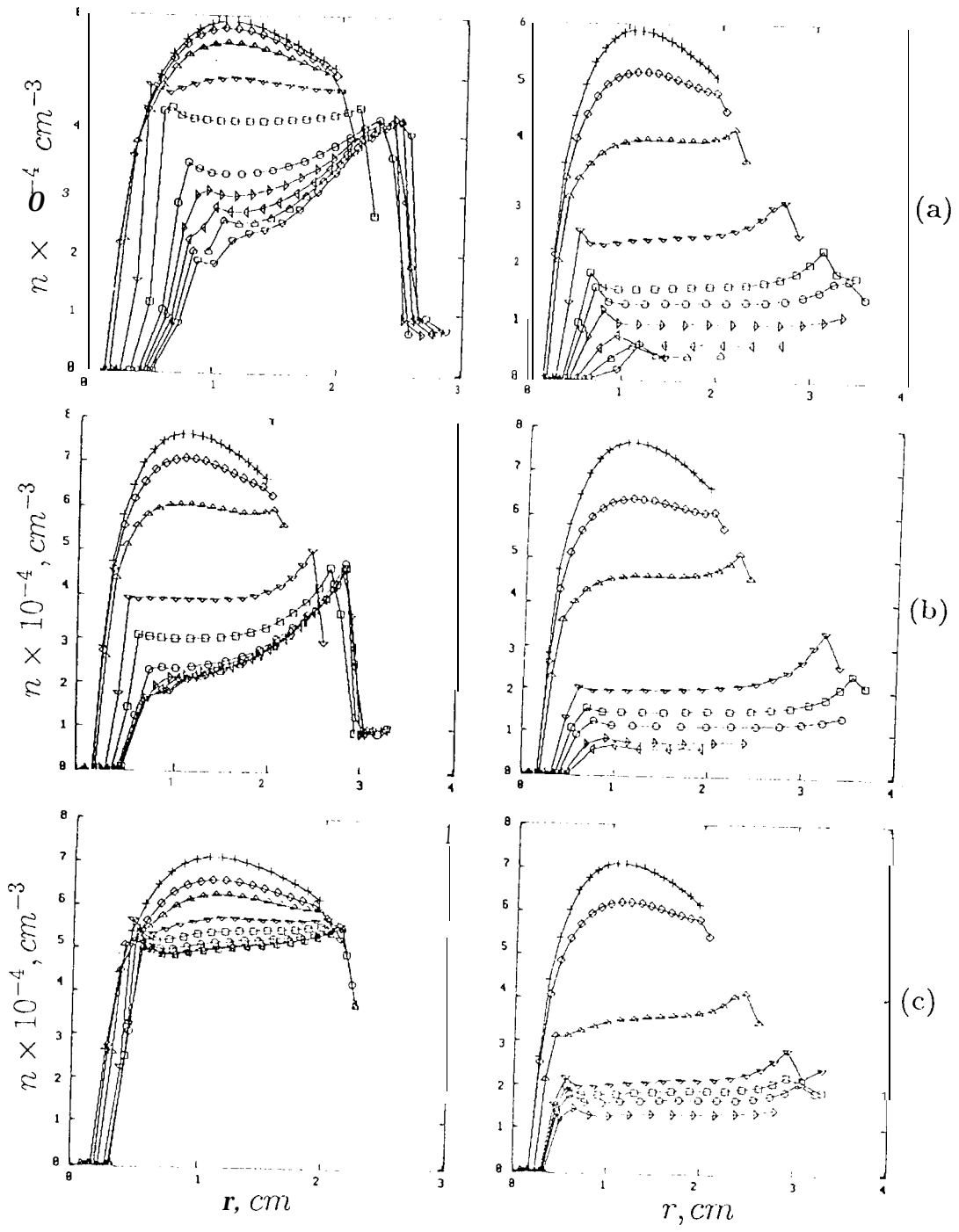
(c)

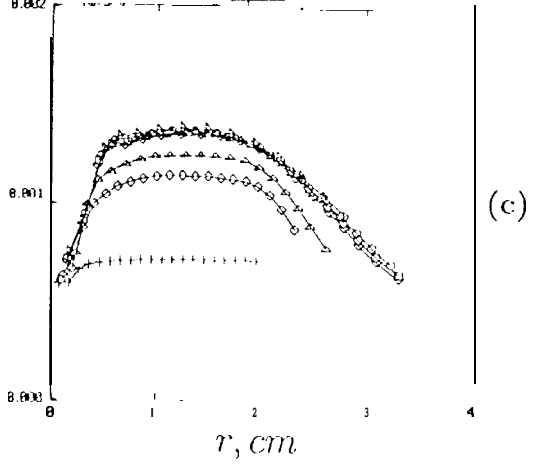
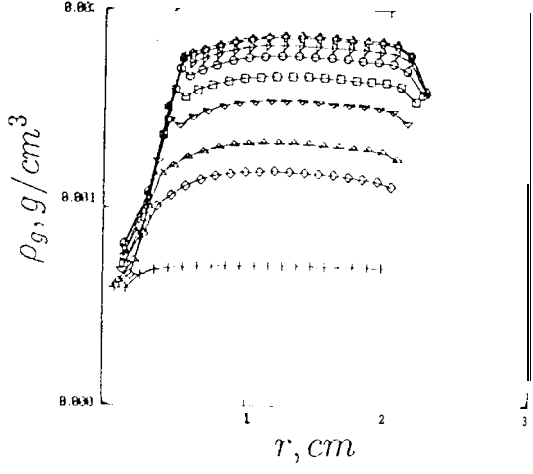
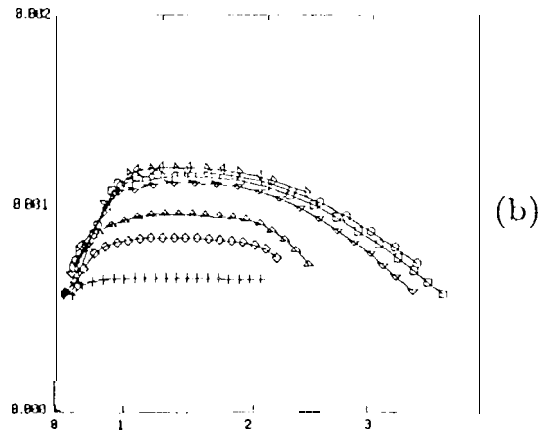
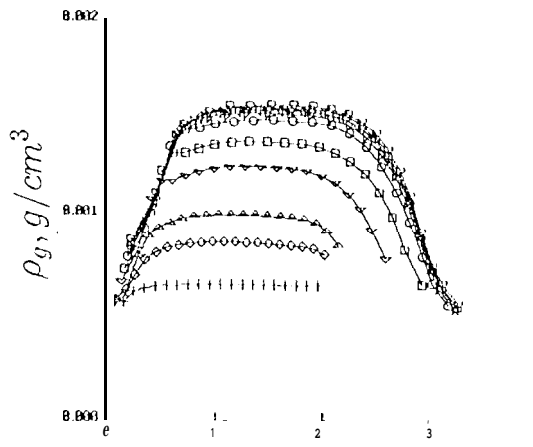
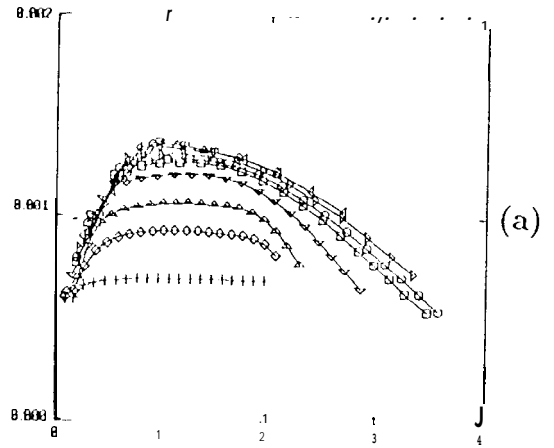
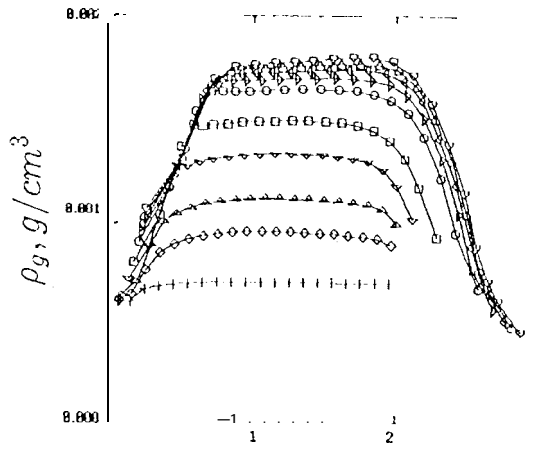


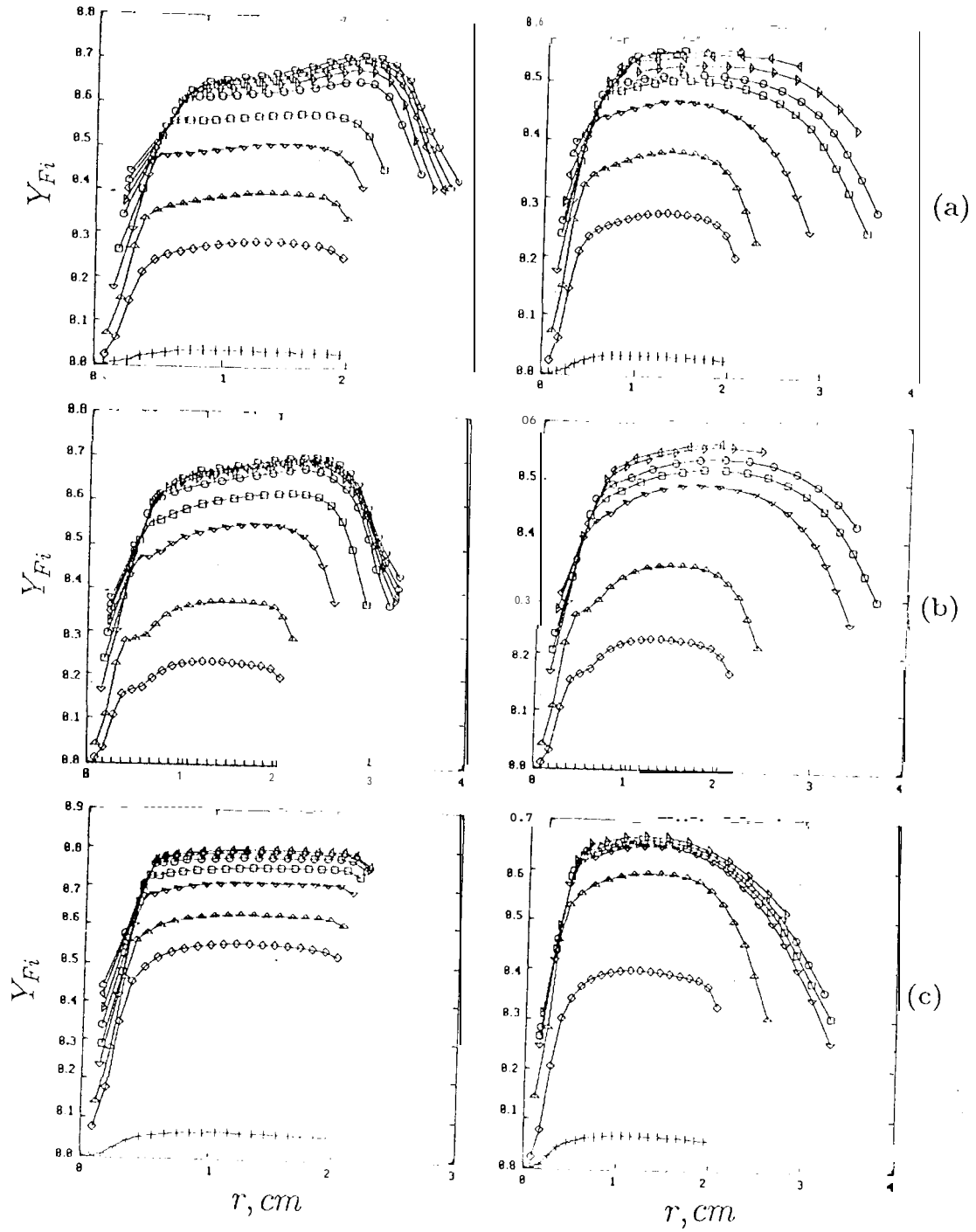
(d)

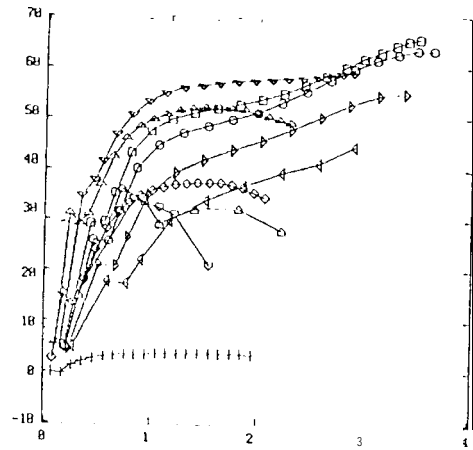
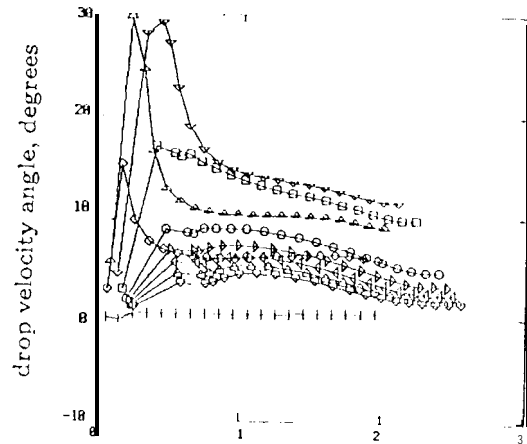




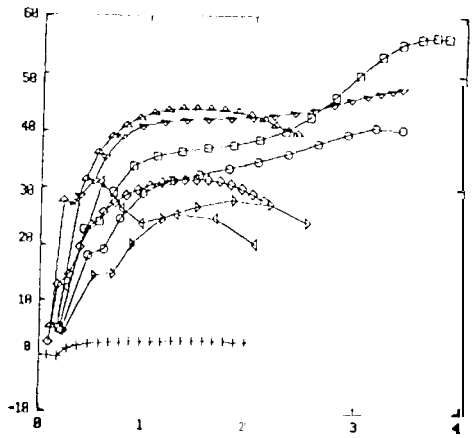
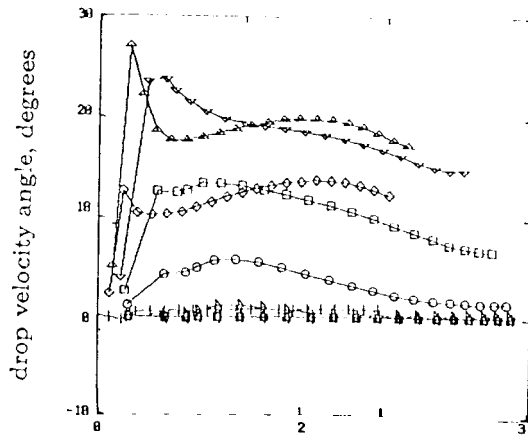




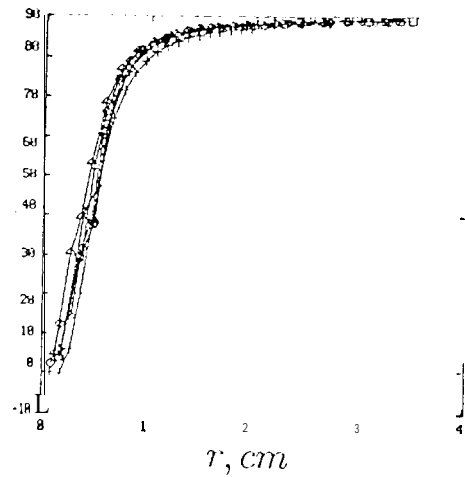
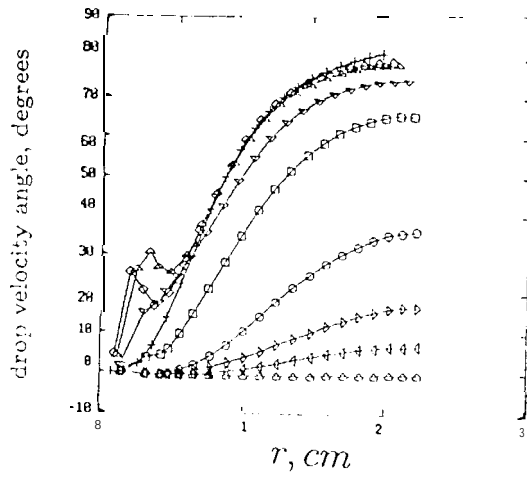




(a)



(b)



(c)